Article

Conversion of Weathered Coal into High Value-Added Humic Acid by Magnetically Recoverable Fe₃O₄/LaNiO₃ Nanocatalysts under Solid-Phase Grinding Conditions

Manrong Song [1,†]**, Gang Wang** [1,†]**, Yanli Suo** [1]**, Zhiqiang Wu** [2]**, Haijuan Zhan** [1,*] **and Wanyi Liu** [1,*]

1   National Demonstration Center for Experimental Chemistry Education, State Key Laboratory of High-Efficiency Utilization of Coal and Green Chemical Engineering, College of Chemistry and Chemical Engineering, Ningxia University, Yinchuan 750021, China; 18255449032@163.com (M.S.); wanggangnxdx@163.com (G.W.); suoyanli0828@163.com (Y.S.)

2   College of Chemistry and Chemical Engineering, Ningxia Normal University, Guyuan 756001, China; wuzqns@nxnu.edu.cn

*   Correspondence: drzhj1225@126.com (H.Z.); liuwy@nxu.edu.cn (W.L.)

†   These authors contributed equally in this work.

Abstract: The Fe₃O₄/LaNiO₃ composite, synthesised with the sol-gel method, is considered to be an excellent nanocatalyst for the production of high value-added humic acids from oxidised weathered coal under solid phase milling process conditions. Under optimum process conditions (1% catalyst, 10% activator, 60 min grinding), 48.4% of the weathered coal can be oxidised to produce humic acid. The prepared Fe₃O₄/LaNiO₃ catalyst was characterized by HRTEM, XRD, and XPS, etc. The heterojunction structure that can promote the electron transfer between the components of the composite material was formed with the recombination of Fe₃O₄ and LaNiO₃. The activation of surface oxygen species and adsorbed oxygen could be enhanced with the help of electron transfer between components. Compared to the blank sample or the LaNiO₃ catalyst alone, the molecular weight of the humic acid produced using the Fe₃O₄/LaNiO₃ composite catalyst was significantly lower (maximum heavy mean molecular weight decreased from 59.7 kDa to 5.5 kDa) and the number of reactive groups in humic acid increased (to seven times that of the blank sample). Oxygen-free vacuum experiments indicated that O₂ has an indispensable effect on its excellent catalytic performance in the Fe₃O₄/LaNiO₃ system. In addition, Fe₃O₄/LaNiO₃ could be used at least six times by simple magnetic separation. The development and preparation of perovskite composite catalysts provide a promising approach to the environmentally friendly development and application of weathered coal, as well as an effective method to resolve the associated environmental pollution.

Keywords: weathered coal; humic acid; Fe₃O₄/LaNiO₃; magnetically recoverable

1. Introduction

Weathered coal is a kind of waste coal derived from coal mines that has not been used as a useful mineral resource [1–3]. With the exploitation of coal resources, the random stacking of weathered coal causes a great waste of resources and huge pollution of the environment, such as air pollution and surface and underground water contamination [4], but it can be used as a valuable source for the preparation of humic acid materials. The basic structure of humic acid is rich in fatty aromatic and oxygen-containing active functional groups [5–7] (carboxyl group, phenolic hydroxyl group, quinone group, and carbonyl group, etc.), permitting a wide range of applications in agriculture [8,9], soil remediation [10], industry [11,12], and composite material [13] fields, etc. In the past, several studies used HNO₃ [14], KMnO₄ [15], and H₂O₂ [16] oxidants to produce active humic acid in low-rank coal. However, these processes have the disadvantages of requiring a large amount of oxidant, long reaction time, producing significant environmental pollution

and an unrecyclable catalyst. Therefore, the development of low-cost, high-efficiency, and environmentally friendly catalytic oxidation methods for preparing active humic acid is still of great significance. Recent studies have shown that lignite can be activated with heterogeneous catalysts such as Pd/CeO_2 for the preparation of humic acids under solid phase ball milling conditions [17,18]. The preparation of humic acid using a heterogeneous catalyst with a mechanical grinding method has two advantages: Firstly, the high intensity squeezing and collision during mechanical grinding can break the encapsulation and binding of the silicates in the coal sample to the organic matter [19,20]. Secondly, a heterogeneous catalyst with oxidation capacity can oxidatively degrade the large molecular weight organic matter in the coal sample during grinding, thus producing low molecular weight humic acid.

In recent years, among the developed catalysts, perovskite oxide has come to be considered as a promising potential catalyst and has attracted great attention. Perovskite oxide has the advantages of low cost, high mechanical strength, flexible structure, high intrinsic catalytic activity, etc. [21–24]. Perovskite with ABO_3 structure has been widely used in diesel exhaust gas treatment [25], methane and styrene oxidation [26,27], and volatile organic compound oxidation etc. [28]. In particular, the perovskite oxide $LaNiO_3$ is a promising oxygen electrocatalyst for renewable energy storage and conversion technology, because the perovskite alloying step strengthens the Ni 3d-O 2p hybridization and reduces the charge transfer energy, this process enhances the activity of the oxygen evolution reaction [29]. The study also found that the use of perovskite ball milling to synthesize small organic molecules has achieved very valuable results [30]. In addition, it has been reported that the heterojunctions of interface oxides, such as $LaAlO_3/SrTiO_3$ and $MnO_3/LaNiO_3$ [31], are more conducive to charge transfer. However, the production of activated humic acid with $Fe_3O_4/LaNiO_3$ solid-phase activated weathered coal has not been examined. Perovskite materials have been shown to have a strong oxidising capacity and can act as effective catalysts for the oxidative degradation of organic pollutants. The Fe atoms in the Fe_3O_4 material are already in the high valence state and have a certain oxidation capacity of their own. In addition, the most important thing is that the Fe_3O_4 material is magnetic and can be recycled. The combination of Fe_3O_4 material and perovskite materials will greatly reduce the difficulty of catalyst recovery and reduce the cost of the reaction while enhancing the oxidation capacity.

Here, the highly active $Fe_3O_4/LaNiO_3$ as a catalyst for the preparation of active humic acid by solid-phase grinding was first reported. This work aims to investigate the possibility of valorizing humic acid by $Fe_3O_4/LaNiO_3$ solid phase treatment and to examine the physicochemical properties of humic acid after different treatments. In addition, the easy preparation, separation, and regeneration processes together with the high catalytic reactivity seem to make $Fe_3O_4/LaNiO_3$ a promising environmentally friendly catalyst.

2. Results and Discussion

2.1. Characterization of Catalysts

2.1.1. Crystal Structure and Morphology

The XRD patterns of the synthesized $LaNiO_3$, Fe_3O_4, and $Fe_3O_4/LaNiO_3$ catalysts are shown in Figure 1a. It can be seen that the composite $Fe_3O_4/LaNiO_3$ catalyst still maintains the main crystal plane of $LaNiO_3$, such as 101, 110, 202, and 122. In addition, the peak of Fe_3O_4 appeared at 2θ of 35.4°, which also suggests that the $Fe_3O_4/LaNiO_3$ composite material was successfully synthesized. It is important to note that there have been numerous reports in the literature on the offset of crystalline surfaces in metal oxide materials after bonding due to the creation of heterogeneous junction structures. The Bragg equation shows that when Fe^{3+} (r = 0.645 nm) is introduced into the material, it will combine with Ni^{3+} (r = 0.0600 nm) with a smaller ionic radius, leading to an increase in the crystalline spacing of the composite and a shift of the diffraction peak towards a lower angle [32]. A slight shift in the position of the peak at the crystalline plane of (202) was also found in the XRD image of the $Fe_3O_4/LaNiO_3$ composite material in Figure 1b. So, this is

presumed to be due to the formation of a heterojunction in the material composite, and the same conclusion was confirmed by TEM and XPS analysis.
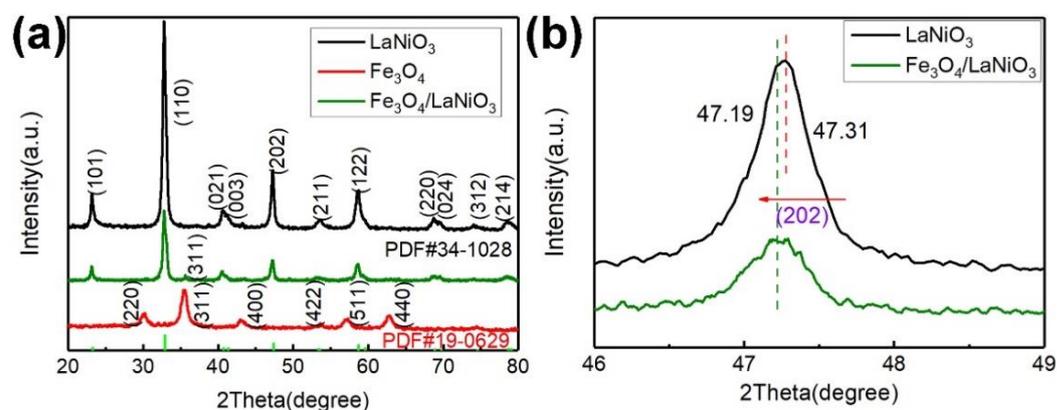

Figure 1. XRD patterns of LaNiO$_3$, Fe$_3$O$_4$ catalyst and Fe$_3$O$_4$/LaNiO$_3$ catalyst: (**a**) full spectrum; (**b**) partial view.

The SEM of the Fe$_3$O$_4$/LaNiO$_3$ catalyst (Figure 2a,b) indicates an irregular morphology, large massive particles, and its surface is relatively smooth, as shown in Figure 2b. The particle size of the nanocomposite material is about 25–130 nm, and its average particle size is about 55 nm. The TEM of the Fe$_3$O$_4$/LaNiO$_3$ catalyst (Figure 2c) also indicates that the heterojunction in the Fe$_3$O$_4$/LaNiO$_3$ composite is formed by the combination of LaNiO$_3$ and Fe$_3$O$_4$, which also proves that LaNiO$_3$ and Fe$_3$O$_4$ are successfully compounded through chemical bonding, rather than simple mixing. In the HR-TEM images of the fresh material (Figure 2d), three lattice stripes with different crystal plane spacing were found and measured, with d = 0.272 and d = 0.381 being attributed to the 110 and 101 crystal planes of the LaNiO$_3$ material. The diffraction intensity of the (110) crystal plane is the strongest among the characteristic peaks of the LaNiO$_3$ material, as can be seen from the XRD images, so the lattice stripes of this crystal plane can be clearly found in the HR-TEM. However, another lattice stripe with d = 0.699 was found in the Fe$_3$O$_4$/LaNiO$_3$ material, and this lattice stripe with crystalline surface spacing is neither a LaNiO$_3$ material nor an oxide of Fe. In addition, a clear interlacing of lattice stripes was found at this site, so the lattice stripes at d = 0.699 were attributed to the heterojunction structure that arises when Fe$_3$O$_4$/LaNiO$_3$ composites are formed by combining Fe$_3$O$_4$ and LaNiO$_3$ materials. It has been reported in the literature that the creation of such heterojunction structures is conducive to the transfer of electrons in the material and would be more conducive to catalytic reactions.

In addition, element mapping from synthesized Fe$_3$O$_4$/LaNiO$_3$ (Figure 2e–i) shows that the density of La and Ni elements in the edge area of the material is greater than that of Fe element, indicating that LaNiO$_3$ in the composite material covers the surface of Fe$_3$O$_4$. At the same time, it can also be observed that the elements of La, Ni, and O are evenly distributed on the surface of Fe$_3$O$_4$, further proving that the Fe$_3$O$_4$/LaNiO$_3$ heterojunction composite material was successfully synthesized.

2.1.2. XPS Analysis

Valence states of constituent elements of the Fe$_3$O$_4$/LaNiO$_3$ catalyst were detected by XPS. The XPS characterization of the Fe$_3$O$_4$/LaNiO$_3$ catalyst is shown in Figure 3a. Although XPS analysis is more accurate as a qualitative analysis, it is also a semi-quantitative method of detection. The percentage atomic contents of the various elements in the Fe$_3$O$_4$/LaNiO$_3$ material that can be obtained from the full spectrum analysis by XPS: La 15.73 at.% (Atomic content%), Ni 14.67 at.%, Fe 1.98 at.%, O 67.63 at.%. The ratio of the number of atoms of Ni to the number of atoms of La is close to 1:1, which corresponds to the ratio of La to Ni in the material. In addition, the atomic content of O obtained by XPS analysis is significantly higher than that of Fe$_3$O$_4$/LaNiO$_3$ (58.3%), due to the presence of

adsorbed oxygen and adsorbed H_2O on the surface of the material. Figure 3b shows the peaks of lanthanum metal in the composite. It can be seen that lanthanum metal shows two peaks at 837.6 eV and 854.5 eV, which are attributed to the characteristic peaks of La 3d 3/2 and La 3d 5/2, respectively, indicating the presence of lanthanum metal in the trivalent form. Of course, it is necessary to compare the XPS spectra of $LaNiO_3$ and $Fe_3O_4/LaNiO_3$ materials to illustrate the effect of the introduction of Fe_3O_4 on the composites. The spectral data for the metals La and Ni are largely unaffected by the Fe element in the XPS spectra, but the energy spectral data for the oxygen element are sensitive to this structural change. For this reason, the spectral data for the oxygen element in both materials were fitted and the results are shown in Figure 3c. The oxygen elements in the diagram can be fitted to four different types: lattice oxygen (O^{2-}), OH^-/CO_3^{2-}, adsorbed (O^-/O_2^-) [33,34], and adsorbed water. After comparison, it can be found that when Fe_3O_4 and $LaNiO_3$ are compounded to form $Fe_3O_4/LaNiO_3$ composites, the lattice oxygen (O^{2-}) content of the composites decreases and the adsorbed oxygen (O^-/O_2^-) content increases. This may be due to the increased specific surface area of the composite material, which can adsorb more oxygen and expose more adsorption sites [35], and the oxygen adsorbed on the catalyst surface forms O^-/O_2^-, which is consistent with the results of BET tests.
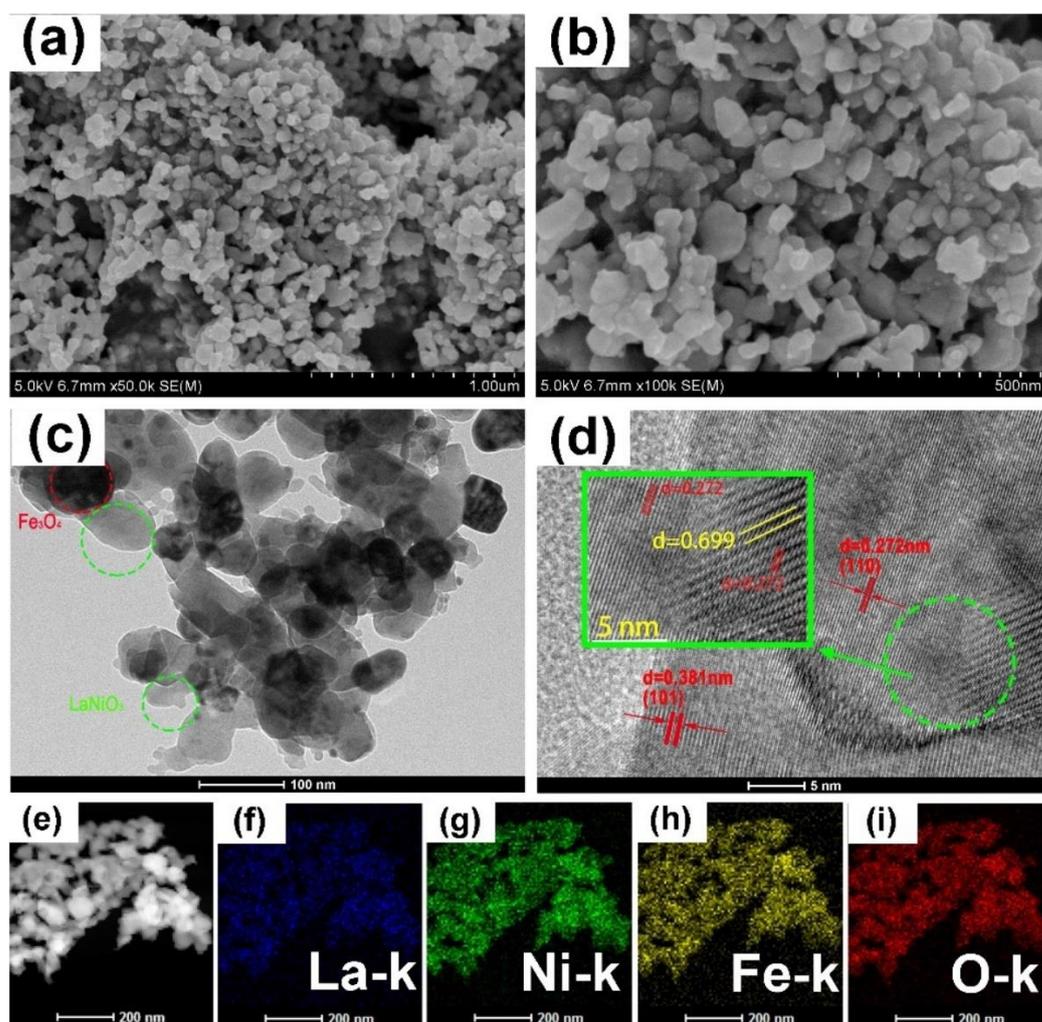
Figure 2. (**a**,**b**) SEM of $Fe_3O_4/LaNiO_3$ catalyst; (**c**,**d**) TEM and HRTEM pictures; (**e–i**) EDX element mapping.
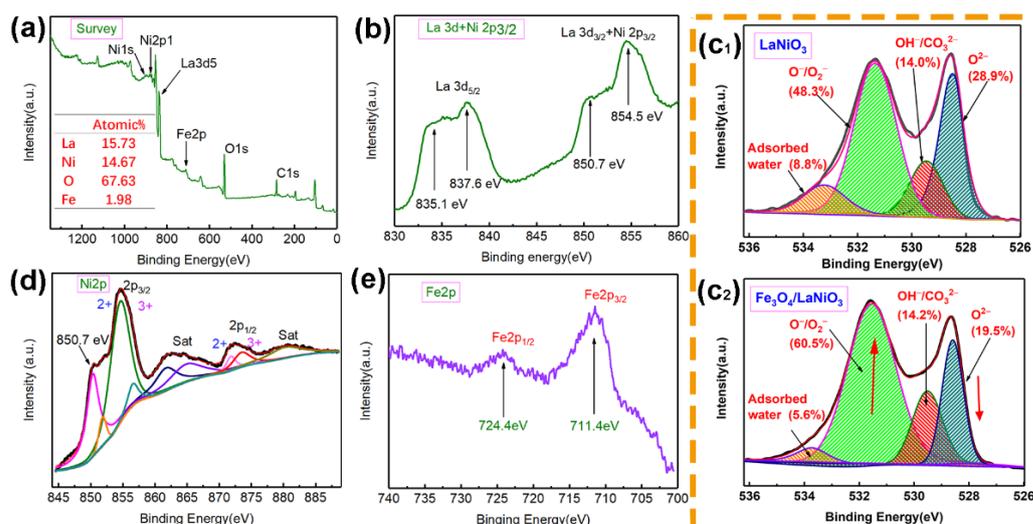
Figure 3. XPS spectrum of $Fe_3O_4/LaNiO_3$ catalyst: (**a**) full spectrum; (**b**) La 3d; (**c**) O 1s; (**d**) Ni 2p; (**e**) Fe 2p.

Figure 3d shows the XPS spectral data for nickel, which shows a number of satellite peaks, although Ni 2p 3/2 and Ni 2p 1/2 peaks can still be found, indicating that nickel is present in both Ni^{2+} and Ni^{3+} forms. In addition, the peaks of 711.4 eV and 724.4 eV in Figure 3e correspond to the electronic layer structures of Fe 2p 3/2 and Fe 2p 1/2 of Fe_3O_4 [36]. These results show that the surface of $Fe_3O_4/LaNiO_3$ has a composition containing La^{3+}, Fe^{2+}, Fe^{3+}, Ni^{2+}, and Ni^{3+} species. It can be found from the spectrum of XPS (Figure 3a,e) that the peak intensity of Fe element is very weak, possibly because part of the surface of Fe_3O_4 nanoparticles is covered by $LaNiO_3$, which masks Fe element to a certain extent. This is consistent with the above XRD, HRTEM, and element mapping information.

2.1.3. N_2 Adsorption−Desorption

Information on the surface area, pore volume, and micropore volume of $LaNiO_3$ and $Fe_3O_4/LaNiO_3$ materials was obtained using N_2 adsorption-desorption measurements (Figure 4). With the data from the BET test, it can be ascertained that the specific surface area of $Fe_3O_4/LaNiO_3$ composite is 12.776 m^2/g, which is 2.2 times that of $LaNiO_3$ alone. The N_2 adsorption-desorption isotherms showed type H3 (Figure 4), indicating that the pore structure is very irregular, which is consistent with the SEM (Figure 2a,b) conclusion. Compared to the $LaNiO_3$ material alone, the improvement in surface area and pore volume of the $Fe_3O_4/LaNiO_3$ composites is across the board. A larger specific surface area is usually more conducive to adsorption contact with the material and will provide more active sites, thus enhancing catalytic performance. Similarly, the increased porosity demonstrates that the material has more pores, which will provide a favorable site for the activation of oxygen in the air to produce active oxygen in the composite.

2.2. Catalytic Performance Evaluation

Humic acid materials have a wide range of applications in agriculture and industry, so the continued development of process routes for the oxidation of weathered coal to humic acid using heterogeneous catalysts is of great research value. The $Fe_3O_4/LaNiO_3$ composites prepared in this paper were used to catalyse the oxidation of weathered coal to produce humic acid under mechanical grinding conditions, and the results of the elemental analysis of the samples are shown in Table 1. WC is the sample obtained from the blank experiment. AWC is the sample with only the addition of sodium hydroxide to assist the grinding. ALC is the sample using $LaNiO_3$ material as the catalyst. AFC is the sample obtained using $Fe_3O_4/LaNiO_3$ composite as the catalyst. From the test results of the elemental analysis in Table 1, it can be found that the humic acid material obtained

using the $Fe_3O_4/LaNiO_3$ composite has the highest elemental O content, indicating that $Fe_3O_4/LaNiO_3$ catalysis has the optimal catalytic capacity to oxidise weathered coal to obtain more oxygen-containing functional groups. It is also noticeable that the H/C ratio decreases and the O/C ratio increases with the addition of catalyst to the different samples. This indicates that more of the hydrocarbons in the material are oxidised to oxygen-containing functional groups [37].
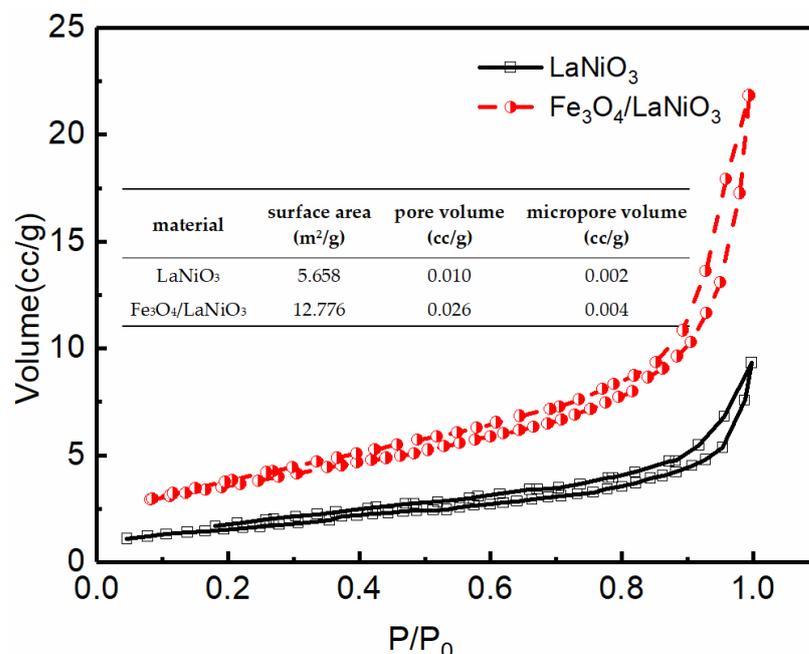

Figure 4. N_2 physical adsorption isotherms for $LaNiO_3$ and $Fe_3O_4/LaNiO_3$ catalysts.

Table 1. Elemental Composition (%), Atomic Ratio Total Humic Acid (%), Water Humic Acid, and E_4/E_6 Ratio of WC, AWC, ALC and AFC.

Sample	Elemental Composition (wt.%)								
	C ad	H ad	O ad	N ad	H/C	O/C	TOC [a]	THA [b]	E_4/E_6 [c]
WC	45.26	3.73	26.28	0.83	0.08	0.58	43.48	32.14	2.38
AWC	40.62	3.31	24.89	0.81	0.08	0.61	42.34	37.65	3.52
ALC	41.46	3.52	23.98	0.80	0.08	0.58	40.01	49.46	5.02
AFC	37.61	2.96	27.85	0.80	0.07	0.74	35.14	48.40	4.94

[a] TOC: total organic content. [b] THA: total humic acids. [c] E_4/E_6: ratio of light absorbance at 465 and 665 nm. ad: The elemental analysis benchmarks all use an analytical base (air-drying base).

As shown in Table 1, compared with the catalyst free (WC), the total humic acid content of the reaction using $LaNiO_3$ (ALC) and $Fe_3O_4/LaNiO_3$ (AFC) catalysts increased by 17.32% and 16.26%, respectively, suggesting that $LaNiO_3$ and $Fe_3O_4/LaNiO_3$ showed excellent catalytic activity for weathered coal catalysis. Previous studies have shown that the ratio of E_4/E_6 decreases as the content of condensed aromatic rings increases [38]. The E_4/E_6 ratio of WC, AWC, ALC, and AFC showed a significantly increasing trend (Table 1), suggesting that humic acid contained a lower average molecular mass than the other treatments. Lower molecular weight products could be obtained. This was further verified by size exclusion chromatography [39]. The molecular weight distribution of humic acid is shown in Figure 5a. The initial HAs matter (WC) was distributed in the range between 70.0 and 5.0 kDa. The high molecular fractions of HAs were lost after ALC and AFC treatments, either by fragmentation into smaller molecules or by being polymerized into the other small molecule products.
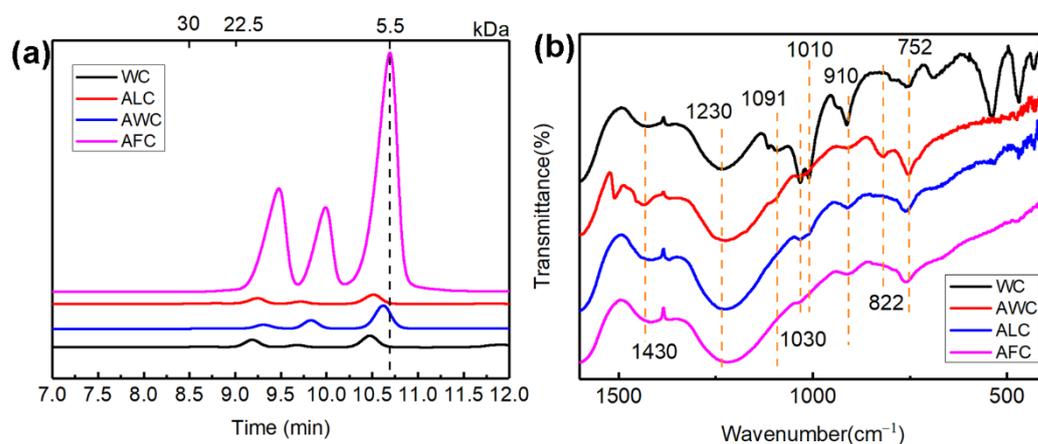
Figure 5. Humic acid molecular weight distribution (**a**) and IR (**b**) spectra of four different treatments.

Compared with the blank samples (WC), the products obtained by adding an activator (NaOH, AWC) and catalyst ($LaNiO_3$, ALC) to the grinding process had smaller molecular weights and narrower distributions. It is worth noting that by adding $Fe_3O_4/LaNiO_3$ catalyst to the weathered coal sample, the maximum average molecular weight is about 5.5 kDa, accounting for 75.0%, and the average molecular weight is 10.0 kDa, accounting for 25.0%. The molecular weight is lower and the distribution is concentrated, indicating that the catalyst $Fe_3O_4/LaNiO_3$ oxidizes the macromolecule humic acid in coal to a much lower molecular weight product. This shows that the use of $Fe_3O_4/LaNiO_3$ catalyst for the catalytic weathering of coal humic acid is very effective.

FTIR was used to detect functional group changes in four different treatments of humic acid. Figure 5b shows that the functional group of humic acid contains characteristic peaks of aromatic rings, namely -OH, COO-, C-O-, etc. [40,41]. After ALC and AFC, the peak displays almost no change in the region between 1700 and 1600 cm^{-1} (Figure 5b). However, the characteristic peaks at 1430 cm^{-1} and 1230 cm^{-1} were shifted toward low wavenumbers, and the characteristic peaks at 752 cm^{-1} were shifted toward high wavenumbers (Figure 6b). This suggests the appearance of groups that resonate in this region, such as COO-, C-O-, and COOH (1420 cm^{-1}), as well as sp^3-CH_2 and benzene ring (766 cm^{-1}). This further indicates that $Fe_3O_4/LaNiO_3$ catalyzes macromolecules in weathered coal to be benzene ring active products. In addition, the characteristic peaks at 1091, 1030, 1010, and 650–400 cm^{-1} disappear, suggesting that the main ash composition in coal samples is Si-O. The Al-O-Si functional group structure disappears after activation, which also shows that the activator NaOH can release the humic acid combined with inorganic silicon aluminum and the like in the weathered coal, which is beneficial to the catalytic oxidation and separation of the catalyst. These observations are consistent with previous research conclusions [42,43].

To further demonstrate the functional group changes in samples, XPS analysis of humic acid was conducted. Peak assignments in the XPS were based on previous XPS studies examining HAs [44,45]. XPS was used to determine the relative distribution of functionality in weathered coal humic acid. Regarding the relative content of carbon-containing functionalities in the C 1s spectrum, the four chemical states are fitted to obtain the fitting line of C 1s (Figure 6). Related components: (1) unsubstituted aromatic carbon and (290–291 eV). This indicates that there is a mixture of aromatic C, C-O-, C=O, and COO- on the surface of HA. These mixtures are related to the functional groups previously identified by HAs [45], and these results are also directly proven by FTIR (1420 cm^{-1}, 1220 cm^{-1}) (Figure 5b). Under the $LaNiO_3$ (ALC) and $Fe_3O_4/LaNiO_3$ (AFC) catalysts, the content of aromatic C increased by 15.50% and 9.34%, respectively, compared to WC, while the carboxyl C content also increased (Table 2). This is consistent with the conclusion of elemental analysis that ALC and AFC humic acids have an increased aromatic structure. Moreover, this shows that catalytic redox produces more aromatic structures and active functional group products.
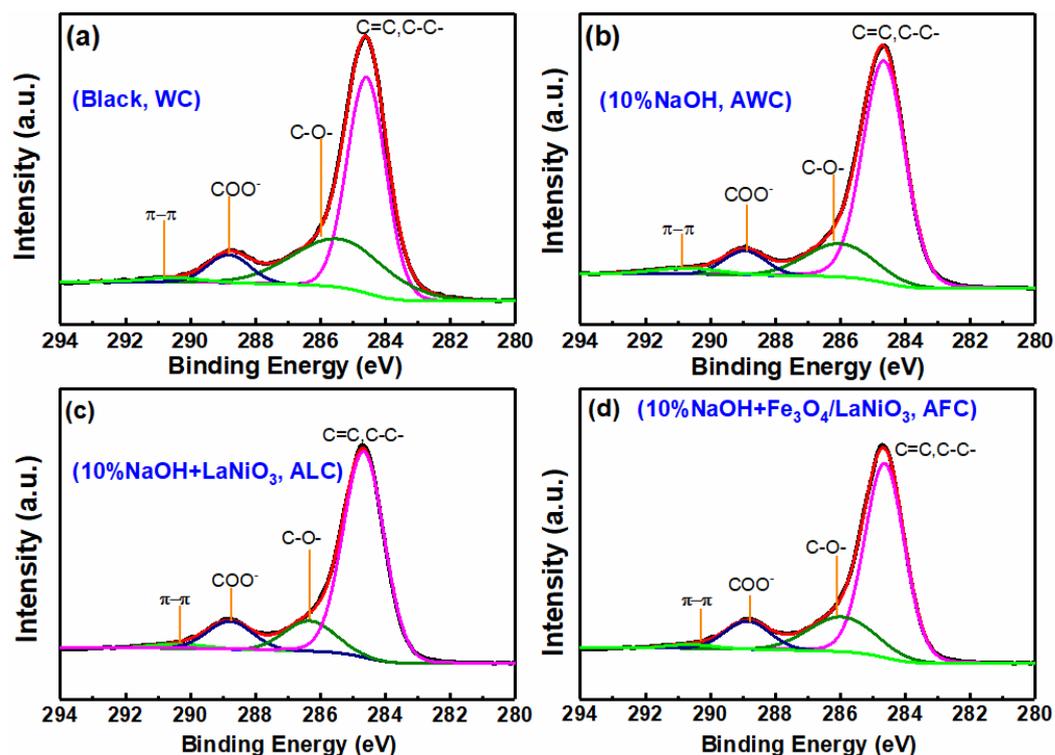
Figure 6. XPS C 1s spectra of four different treatments of humic acid (**a**) WC, (**b**) AWC, (**c**) ALC, and (**d**) AFC.

Table 2. Relative distribution of carbon functional groups in weathered coal humic acid determined by XPS.

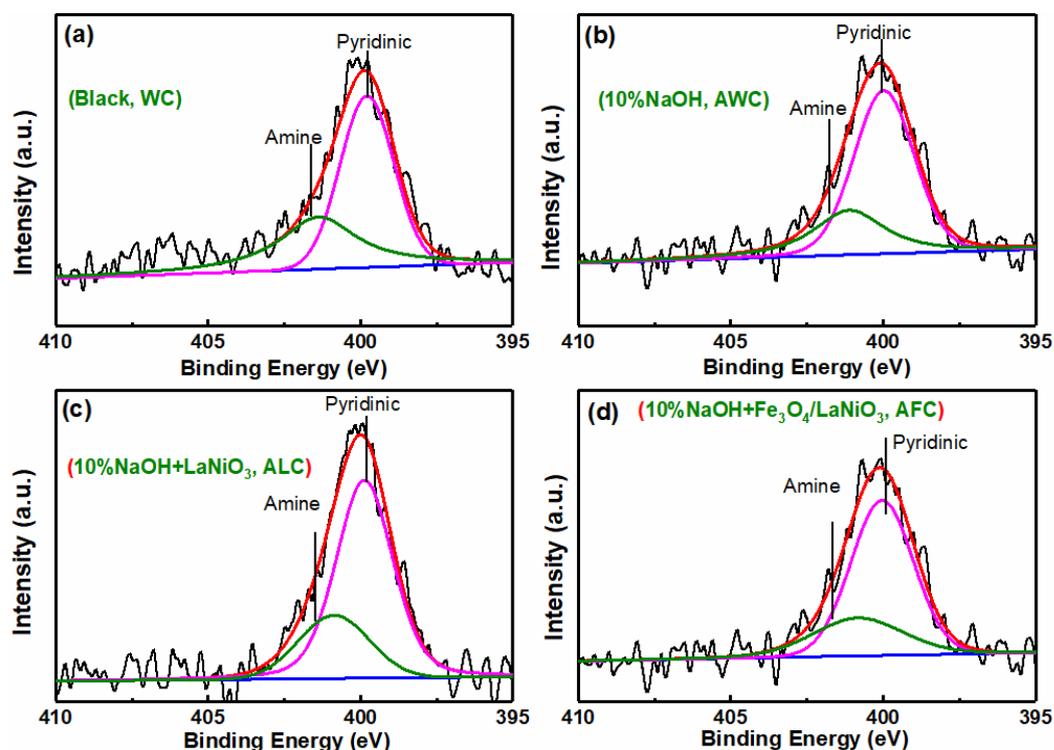| Weathered Coal	Aromatic		Ether/Alcohol		Carboxylic		π-π *	
	BE [a]	RP [b]	BE [a]	RP [b]	BE [a]	RP [b]	BE [a]	RP [b]
WC	284.6	58.98	285.4	31.31	288.8	8.15	290.5	1.56
AWC	284.6	63.18	285.5	26.54	289.0	7.63	290.8	2.65
ALC	284.7	74.48	286.3	12.90	288.8	12.51	290.4	1.89
AFC	284.6	68.32	286.0	19.72	288.9	10.58	290.6	1.38

[a] BE, binding energy (eV); [b] RP, relative proportion (in%) of each functional group corresponding to fitted curves in Figure 6. * π-π conjugate structure.

Weathered coal humic acid contains nitrogen in the form of amine groups and pyridine. N 1s spectroscopy confirmed that the four differently processed samples contained large concentrations of amine groups and pyridine N (Figure 7). The previous literature reports that there are amine groups and pyridine N in humic acid [44]. The quantitative relative content was quantified by fitting. The results showed that after adding the activator NaOH, the pyridine N content increased while the amine N content decreased (Table 3). This may be because the activator breaks the coordination bond between N and inorganic metals, such as Si and Al. These changes can be supported by the FTIR fingerprint region. After activation and catalysis, electron transfer may be split into smaller molecules and then polymerized to form pyridine and other substituent small molecule products.

Table 3. Relative distribution of oxygen and nitrogen functional groups in weathered coal humic acid by XPS.

Weathered Coa	Oxygen						Nitrogen			
	C-O-		C=O		H_2O		Pyrrole		Ammonium	
	BE [a]	RP [b]	BE [a]	RP [b]	BE [a]	RP [b]	BE [a]	RP [b]	BE [a]	RP [b]
WC	531.8	54.78	533.2	39.53	534.9	5.69	399.8	60.37	401.4	39.63
AWC	531.8	44.47	533.3	54.76	535.5	0.77	400.0	70.12	401.1	29.88
ALC	531.6	44.14	533.2	55.29	535.8	0.58	399.9	73.82	400.9	26.18
AFC	531.7	47.73	533.3	49.58	535.0	2.68	400.0	72.36	400.8	27.64

[a] BE, binding energy (in eV); [b] RP, relative proportion (in%) of each functional group corresponding to fitted curves in Figures 7 and 8.

Figure 7. Four different treatments of humic acid XPS N 1s spectrum (**a**) WC, (**b**) AWC, (**c**) ALC, and (**d**) AFC.

Focusing on the shift to O 1s XPS spectra of four different treatments of humic acid (Figure 8), generally, there are two peaks in the O 1s region, which represent the C-O- and C=O organic bonds, respectively [43]. After four different treatments, three peaks were found. The humic acid sample contains peaks with C=O and C-O- bonds, and another smaller peak of H_2O, located at about 535.5 eV. However, the two peaks fitted at C-O- and C=O are shifted after $Fe_3O_4/LaNiO_3$ catalysis (Figure 8d), and the increase of the C=O functional group (Table 3), which correspond to IR (1420 cm^{-1}) results. The results indicated that these groups were formed during the catalytic treatment.
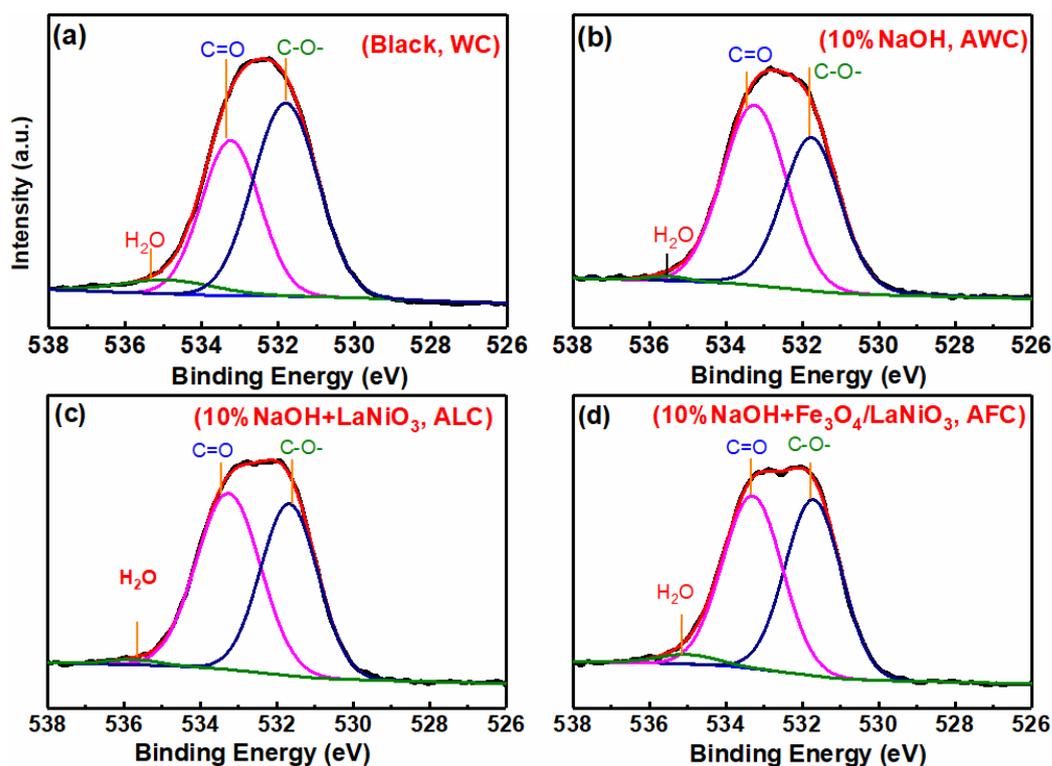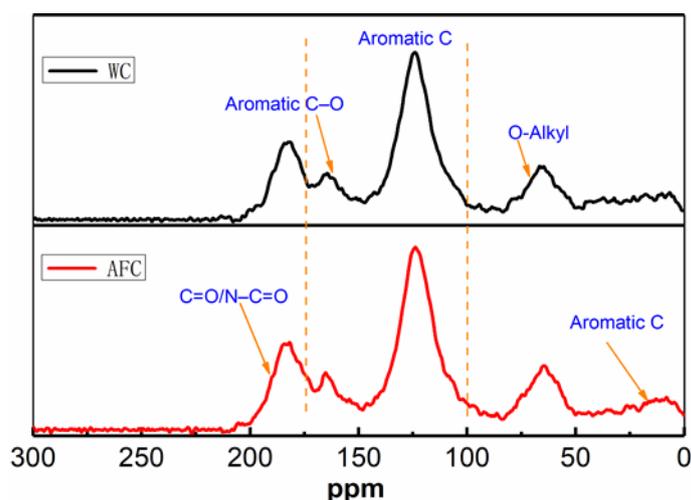
Figure 8. Four different treatments of humic acid XPS O 1s spectrum (**a**) WC, (**b**) AWC, (**c**) ALC, and (**d**) AFC.

The solid ^{13}C NMR spectrum of the humic acid material produced using the $Fe_3O_4/LaNiO_3$ composite (AFC) for catalytic oxidation is shown in Figure 9, and the spectrum can be divided into five main regions: Aliphatic C (0–50 ppm), O-Alkyl (50–100 ppm), Aromatic C (100–150 ppm), Aromatic C-O (150–175 ppm), and C=O/N-C=O (170–220 ppm). Due to the complex molecular structure of humic acid, which contains a variety of functional groups and peaks of different structures overlapping each other, the material obtained after treatment without catalyst (WC) exhibited similar peak patterns in the spectra of solid ^{13}C NMR to the humic acid material (AFC) made by oxidation using the $Fe_3O_4/LaNiO_3$ catalyst. However, after integration calculations, large differences in the contents of the different structural groups in the humic acid materials obtained by the two methods can be found (Table 4). The aliphatic carbon and oxyalkyl contents of the humic acid material obtained using the $Fe_3O_4/LaNiO_3$ catalyst were higher than those of the blank sample without the catalyst, but the content of the aromatic structure was reduced. This suggests that the addition of the catalyst allowed for an enhanced oxidation capacity to oxidatively decompose the large molecular weight aromatic structures into relatively small molecular weight aliphatic structures. In addition, the C-O structure on the aromatic structure is reduced and the C=O/N-C=O structure is slightly increased. This also shows that the addition of the catalyst enhances the ability to oxidise C-O to C=O and other structures. In conclusion, the $Fe_3O_4/LaNiO_3$ catalyst oxidised large molecules to small molecules of compounds containing polycyclic aromatic hydrocarbons, aliphatic hydrocarbons, and polyfunctional groups.

Table 4. Percentage distribution of carbon in WC and AFC determined by solid-state ^{13}C NMR spectroscopy.

Functional Groups	Chemical Shift (ppm)	Area (%)	
		AFC	WC
Aliphatic C	0–50	7.45	6.86
O-Alkyl	50–100	13.83	11.42
Aromatic C	100–148	53.19	57.14
Aromatic C-O	148–170	3.72	4.57
C=O/N-C=O	170–220	21.81	20.0

Area (%): Area of each component/total area after integration by NMR software.

Figure 9. Solid-state ^{13}C NMR spectra of WC and AFC samples.

The humic acid samples obtained by catalytic oxidation using $Fe_3O_4/LaNiO_3$ composites and the samples obtained by blank grinding were tested by GC-MS and the results are shown in Table 5. Because humic acids have a complex structure and are mostly of large molecular weight, only a fraction of the relatively small molecular weight active substances can be detected using GC-MS testing. Seventeen of the substances were detected in the AFC samples compared to only 12 in the WC samples. In addition, the molecular weights of the substances detected in the AFC samples were concentrated in a smaller interval. The quality of the humic acid product can usually be judged by the amount of the small molecules' reactive groups of humic acid. The higher the number of reactive groups, the higher the value of the humic acid. The results of the GC-MS tests showed that the humic acid samples obtained by catalytic oxidation using $Fe_3O_4/LaNiO_3$ composites under solid phase grinding conditions had more reactive groups and were of higher value.

Table 5. GC-MS test results for AFC samples ($Fe_3O_4/LaNiO_3$) and WC samples (Blank experiment).

No.	Molecular Formula	Chemicals (Name) [a]	WC	AFC
1	$C_2H_4O_2$	Acetic acid	✓	✓
2	$C_2H_4O_2$	Methyl formate		✓
3	$C_{10}H_{14}N_2O_4$	2-(2,5-dimethoxy-4-nitrophenyl)ethan-1-amine	✓	
4	C_3H_7NO	Acetaldehyde, O-methyloxime		✓
5	$C_6H_{11}NO_3$	2-Aminoethanol, N,O-diacetyl-		✓
6	$C_7H_{12}N_2$	1-Butylimidazole		✓
7	C_3H_5NO	Propanenitrile, 2-hydroxy-		✓
8	$C_{17}H_{34}O_2$	Hexadecanoic acid, methyl ester	✓	
9	$C_{16}H_{32}O$	2-Hexadecanone		✓
10	$C_{16}H_{22}O_4$	Dibutyl phthalate		✓
11	$C_{19}H_{38}O_2$	Methyl stearate	✓	✓

Table 5. *Cont.*

No.	Molecular Formula	Chemicals (Name) [a]	WC	AFC
12	$C_5H_8N_2$	3,5-Dimethylpyrazole		✓
13	C_6H_8O	4-Methyl-2H-pyran		✓
14	$C_{18}H_{33}N$	9-Octadecenenitrile, (Z)-		✓
15	$C_6H_{10}N_2O$	3,5-Dimethylpyrazole-1-methanol	✓	
16	$C_{16}H_{32}O_2$	n-Hexadecanoic acid	✓	
17	$C_{23}H_{44}O_2$	13-Docosenoic acid, methyl ester, (Z)-		✓
18	$C_{22}H_{41}N$	(Z)-Docos-9-enenitrile	✓	
19	$C_{17}H_{32}O$	13-Heptadecyn-1-ol		✓
20	$C_{18}H_{31}N$	11-Octadecynenitrile	✓	
21	$C_{20}H_{38}O_2$	Ethanol, 2-(9,12-octadecadienyloxy)-, (Z,Z)-		✓
22	$C_{20}H_{39}N$	Eicosanenitrile	✓	
23	$C_{24}H_{38}O_4$	Bis(2-ethylhexyl) phthalate		✓
24	$C_{18}H_{33}N$	9-Octadecenenitrile, (Z)-	✓	
25	$C_{24}H_{38}O_4$	1,4-Benzenedicarboxylic acid, bis(2-ethylhexyl) ester	✓	
26	$C_{22}H_{43}NO$	13-Docosenamide, (Z)-		✓
27	$C_{35}H_{62}O_3$	Benzenepropanoic acid, 3,5-bis(1,1-dimethylethyl)-4-hydroxy-, octadecyl ester	✓	

[a.] Substance analysis referenced to Mass Spectrometry Library Database (NIST17.L).

Further analysis of weathered coal humic acids from different treatments was carried out using thermal cracking gas chromatography-mass spectrometry (PY-GCMS) and the chromatograms are shown in Figure 10. Hence, it can be seen that the samples without catalyst (WC, grinding only) show fewer characteristic peaks and are concentrated in the regions of higher molecular weight. However, the samples treated with the $Fe_3O_4/LaNiO_3$ catalyst (AFC) showed more characteristic peaks of the compounds and significantly more characteristic peaks in the small molecular weight region, in agreement with the results of the SEC tests. These phenomena suggest that the addition of a catalyst to the grinding effectively activates the weathered coal, allowing more humic acid molecules to escape the silicates in the coal sample. In addition, an increase in the number of functional group species containing oxygen in the samples after the addition of the $Fe_3O_4/LaNiO_3$ catalyst can also be found. This indicates that the addition of the catalyst effectively activated the oxygen. Moreover, catalytic oxidation can occur with large molecular weight substances, and smaller molecular weight reactive groups are obtained. Overall, the $Fe_3O_4/LaNiO_3$ composites showed excellent catalytic oxidation performance in the activation of weathered coal to produce humic acid under solid phase grinding conditions, with a significant increase in the content of small molecular weight reactive groups in the produced humic acid material.

Similarly, one of the criteria for evaluating the efficiency of catalyst is the recycled property of the catalyst. We evaluated the recycling performance of the $Fe_3O_4/LaNiO_3$ catalyst for six times (Figure 11). During the initial catalyst cycle experiments, the catalyst is recovered by magnetic separation, rinsed with water and ethanol, dried, and taken directly to the next cycle. The catalytic performance of the catalyst was significantly reduced in the first and second cycles, presumably due to some of the pore structures in the catalyst being blocked by humic acid molecules during the grinding process. Because of the large molecular weight and complex structure of the humic acid material, a simple rinse was not able to completely remove these residues. To test this suspicion, the used catalyst was placed in an ultrasonic cleaner for 30 min, dried, and put into the next cycle. The experimental results show that the catalysts recovered their catalytic capacity after ultrasonic cleaning and were essentially indistinguishable from the first use. In addition, the data obtained from each experiment using the ultrasonically treated material were more stable. However, considering the time and money spent on cleaning the catalyst with each ultrasonic treatment, we believe that the experimental results obtained with both treatment options are meaningful and that others may choose to use them depending on the situation.
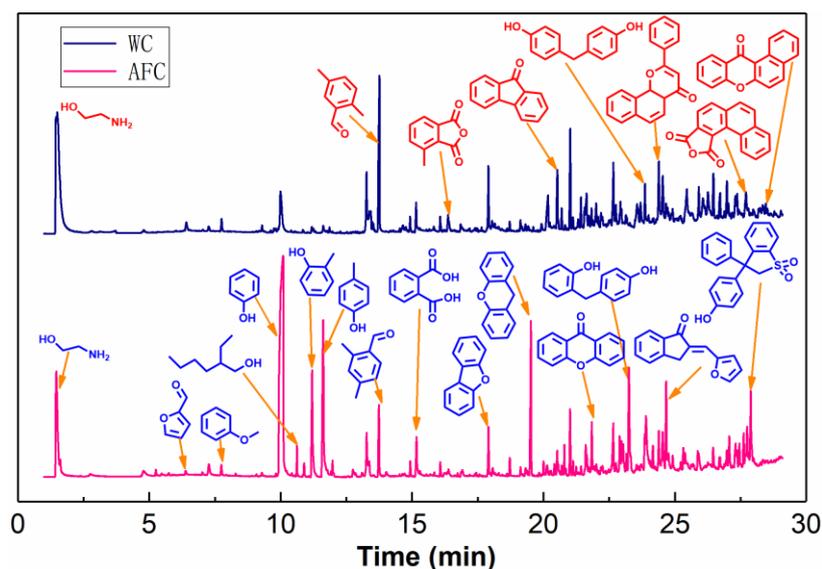
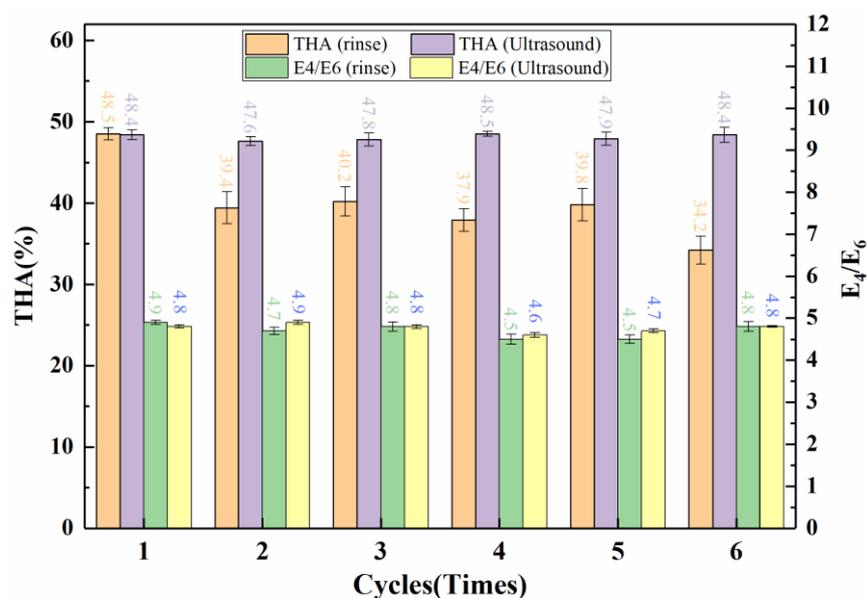**Figure 10.** Thermal cracking gas chromatography-mass spectrometry (PY-GCMS) of AFC and WC samples.

Figure 11. Recycling performance of $Fe_3O_4/LaNiO_3$ catalyst.

2.3. Mechanism Analysis

The $Fe_3O_4/LaNiO_3$ material has been shown to be an excellent catalyst for the catalytic oxidation of weathered coal to humic acid under solid phase grinding conditions. The catalytic mechanism is shown in Figure 12. Firstly, since weathered coal contains a large number of inorganic silicates, the addition of sodium hydroxide during the grinding process can effectively promote the cracking of the silicates, thus releasing more humic acid molecules. The humic acid material obtained at this time has a large molecular weight and contains fewer oxygen functional groups. Secondly, the special electronic structure of the $Fe_3O_4/LaNiO_3$ material effectively activates the oxygen in the air and transforms it into active oxygen molecules adsorbed on the surface (The large molecular weight of humic acid material obtained under vacuum conditions proves that oxygen in air is necessary). These reactive oxygen molecules will then react with the large molecules of humic acid material exposed by the cracking of weathered coal under the action of grinding [46]. Under the action of oxidation and mechanical forces, some of the chemical bonds in the large

molecular weight humic acid material are broken to obtain the final product. The resulting humic acid material has the advantage of being small in molecular weight, high in oxygen functional groups, and high in activity. In addition, comparative experiments showed that the use of the Fe_3O_4/$LaNiO_3$ catalyst gave 48.5% humic acid with >75% of small molecules. These results are significantly better than the data obtained using the $LaNiO_3$ catalyst alone. Thus, the introduction of Fe_3O_4 not only allows the composite catalyst to be recovered by simple magnetic separation, but also adjusts the electronic structure of the $LaNiO_3$ material and increases the reactive sites.

Figure 12. The mechanisms for the oxidation of weathered coal by Fe_3O_4/$LaNiO_3$ catalysts to obtain humic acids.

3. Materials and Methods

3.1. Materials and Characterizations

3.1.1. Materials

$Ni(NO_3)_3 \cdot 6H_2O$ was purchased from Ailan Chemical Technology Co., Ltd. (Shanghai, China). $Ni(NO_3)_3 \cdot 6H_2O$ and $FeCl_2 \cdot 4H_2O$ were purchased from Tianjin Damao Chemical Reagent Factory (Tianjin, China). Citric acid and NaOH were purchased from Tianjin Fengchuan Chemical Reagent Technology Co., Ltd.(Tianjin, China). $FeCl_3 \cdot 6H_2O$ was purchased from Shanghai Guangnuo Chemical Technology Co., Ltd. (Shanghai, China). All materials were analytically pure. The other reagents and solvents used in this study were of analytical reagent grade and were not purified further.

3.1.2. Characterizations

The samples were analysed using the following instruments: XRD (Bruker-AXS Co., Billerica, German); SEM (FESEM, S-4800, Hitachi, Japan); TEM (Tecnai G2 F30, Hillsboro, OR, USA); XPS (Thermo escalab 250Xi); BET (QuadraSorb SI, Tallahassee, FL, USA); GC-MS (QP2010-SE); PyGC-MS (PY-3030D/7890B-5977A); solid-state ^{13}C NMR (Agilent 600M, Sacramento, CA, USA).

3.2. Catalyst Preparation

3.2.1. Synthesis of $LaNiO_3$ Catalysts

$La(NO_3)_3 \cdot 6H_2O$ (10 mmol), $Ni(NO_3)_3 \cdot 6H_2O$ (10 mmol) and citric acid (20 mmol) were added to a beaker. Then, 20 mL each of deionised water and ethanol were added. After the sample was completely dissolved, it was heated to 80 °C and the solvent was evaporated to form a gel. The samples were dried and transferred to a muffle furnace for calcination, with a temperature rise procedure [26]: 25–170 °C (3 °C/min), kept for 2 h; 170–500 °C (3 °C/min), kept for 4 h; 500–700 °C (3 °C/min), kept for 6 h.

3.2.2. Synthesis of Fe_3O_4/$LaNiO_3$ Catalysts

The Fe_3O_4/$LaNiO_3$ (FLNO) catalysts were synthesized using a sol-gel method [47]. Here, the prepared Fe_3O_4 (500 mg) was weighed and dispersed in 250 mL of ethanol

aqueous solution (volume ratio 1/2) by ultrasound. After sonication at room temperature for 6 h, 10 mmol La(NO$_3$)$_3$·6H$_2$O, Ni(NO$_3$)$_3$·6H$_2$O and citric acid were added to the above solution under stirring conditions. The subsequent methods and operations are the same as for the preparation of LaNiO$_3$ sample.

3.3. Catalytic Activity Tests

Briefly, 2.0 g weathered coal sample (80 mesh) and 0.02 g prepared catalyst were placed in a mortar (the mass ratio of weathered coal to catalyst is 100:1) and ground for a certain time at room temperature with the solid NaOH as the activation agent. Inspection by typical single factor and orthogonal experiments mainly included the following three treatments: (1) 10% NaOH activation agent with weathered coal (AWC), (2) 10% NaOH activation agent and 1% LaNiO$_3$ catalyst with weathered coal (ALC), and (3) 10% NaOH activation agent and 1% Fe$_3$O$_4$/LaNiO$_3$ catalyst with weathered coal (AFC). At the same time, weathered coal without activator and catalyst was used as a control (WC). The above experiments were completed by grinding in a mortar for 60 min. Humic acid was extracted from weathered coal based on previous research [16], and the product was then freeze-dried.

For each treated sample (WC, AWC, ALC, AFC), the element content was analyzed by an element analyzer. The content of total humic acid was determined according to a method from previous literature [17,48]. The E$_4$/E$_6$ ratio was determined using a dual-beam ultraviolet-visible spectrophotometer, before 10 mg of prepared humic acid was added to 10 mL of 0.05 mol/L NaHCO$_3$ solution. The absorbance of humic acid was measured at 465 nm and 665 nm, and the E$_4$/E$_6$ ratio was then calculated [33]. The molecular size distribution range of the humic acid was determined by the size exclusion chromatography method. The relative distribution content of active functional groups in humic acid was determined by X-ray photoelectron spectroscopy.

4. Conclusions

In summary, we reported that the nanocatalyst Fe$_3$O$_4$/LaNiO$_3$ synthesized by the sol-gel method has a high catalytic activity for the conversion of weathered coal to active humic acid owing to its heterojunction architectures and high activity of surface oxygen. The interfacial oxide heterojunction Fe$_3$O$_4$/LaNiO$_3$ has stronger catalytic performance than the non-heterojunction catalyst LaNiO$_3$, which was confirmed under solid-phase grinding. By using Fe$_3$O$_4$/LaNiO$_3$ composites as catalysts and weathered coal as raw material, 48.5% humic acid material can be obtained by mechanical ball milling at room temperature for 1 h, where the content of small molecules of active humic acid (5.5 kDa) increases to 75%. In addition, Fe$_3$O$_4$/LaNiO$_3$ is an environmentally friendly catalyst that can be recycled. Overall, this study provides a possible new way for converting weathered coal into active humic acid under mild conditions, and it may provide some enlightenment for the application of the interfacial oxide heterojunction to the solid-phase milling reaction.

References

1. Song, J.-J.; Deng, J.; Zhao, J.-Y.; Zhang, Y.-N.; Shu, C.-M. Comparative analysis of exothermic behaviour of fresh and weathered coal during low-temperature oxidation. *Fuel* **2021**, *289*, 119942. [CrossRef]
2. Kim, J.H.; Chang, B.; Kim, B.J.; Park, C.; Goo, J.Y.; Lee, Y.J.; Lee, S. Applicability of weathered coal waste as a reactive material to prevent the spread of inorganic contaminants in groundwater. *Environ. Sci. Pollut. Res.* **2020**, *27*, 45297–45310. [CrossRef] [PubMed]
3. Guo, H.; Li, Y.; Wang, Q.; Zhao, W.; Jia, J.; Lv, J.; Liu, S.; Xia, D. Feasibility analysis of the in situ conversion of biomethane in surface weathered coal. *Fuel* **2020**, *268*, 117273. [CrossRef]
4. Yenilmez, F.; Kuter, N.; Emil, M.K.; Aksoy, A. Evaluation of pollution levels at an abandoned coal mine site in Turkey with the aid of GIS. *Int. J. Coal Geol.* **2011**, *86*, 12–19. [CrossRef]
5. Abakumov, E.V.; Cajthaml, T.; Brus, J.; Frouz, J. Humus accumulation, humification, and humic acid composition in soils of two post-mining chronosequences after coal mining. *J. Soil. Sediments* **2012**, *13*, 491–500. [CrossRef]
6. Sarlaki, E.; Sharif Paghaleh, A.; Kianmehr, M.H.; Asefpour Vakilian, K. Valorization of lignite wastes into humic acids: Process optimization, energy efficiency and structural features analysis. *Renew. Energy* **2021**, *163*, 105–122. [CrossRef]
7. Zhang, S.; Su, J.; Ali, A.; Zheng, Z.; Sun, Y. Enhanced denitrification performance of strain YSF15 by different molecular weight of humic acid: Mechanism based on the biological products and activity. *Bioresour. Technol.* **2021**, *325*, 124709. [CrossRef]
8. Calvo, P.; Nelson, L.; Kloepper, J.W. Agricultural uses of plant biostimulants. *Plant Soil* **2014**, *383*, 3–41. [CrossRef]
9. Zhang, S.-Q.; Yuan, L.; Li, W.; Lin, Z.-A.; Li, Y.-T.; Hu, S.-W.; Zhao, B.-Q. Effects of urea enhanced with different weathered coal-derived humic acid components on maize yield and fate of fertilizer nitrogen. *J. Integr. Agr.* **2019**, *18*, 656–666. [CrossRef]
10. Pittarello, M.; Busato, J.G.; Carletti, P.; Dobbss, L.B. Possible developments for ex situ phytoremediation of contaminated sediments, in tropical and subtropical regions—Review. *Chemosphere* **2017**, *182*, 707–719. [CrossRef]
11. Sun, Z.; Tang, B.; Xie, H. Treatment of Waste Gases by Humic Acid. *Energy Fuels* **2015**, *29*, 1269–1278.
12. Salati, S.; Papa, G.; Adani, F. Perspective on the use of humic acids from biomass as natural surfactants for industrial applications. *Biotechnol. Adv.* **2011**, *29*, 913–922. [PubMed]
13. Xiao, Z.; Zhou, H.; Hao, J.; Hong, H.; Song, Y.; He, R.; Zhi, K.; Liu, Q. A novel and highly efficient Zr-containing catalyst based on humic acids for the conversion of biomass-derived ethyl levulinate into gamma-valerolactone. *Fuel* **2017**, *193*, 322–330. [CrossRef]
14. Zhumanova, M.O.; Usanboev, N.; Namazov, S.S.; Beglov, B.M. Oxidation of brown coal of Angren deposit with a mixture of nitric and sulfuric acids. *Russ. J. Appl. Chem.* **2010**, *82*, 2223–2229. [CrossRef]
15. Fong, S.S.; Seng, L.; Majri, N.B.; Mat, H.B. A Comparative Evaluation on the Oxidative Approaches for Extraction of Humic Acids from Low Rank Coal of Mukah. *J. Braz. Chem. Soc.* **2007**, *18*, 34–40. [CrossRef]
16. Doskočil, L.; Grasset, L.; Válková, D.; Pekař, M. Hydrogen peroxide oxidation of humic acids and lignite. *Fuel* **2014**, *134*, 406–413. [CrossRef]
17. Tang, Y.; Yang, Y.; Cheng, D.; Gao, B.; Wan, Y.; Li, Y.C. Value-Added Humic Acid Derived from Lignite Using Novel Solid-Phase Activation Process with Pd/CeO$_2$ Nanocatalyst: A Physiochemical Study. *ACS Sustain. Chem. Eng.* **2017**, *5*, 10099–10110. [CrossRef]
18. Tang, Y.; Hou, S.; Yang, Y.; Cheng, D.; Gao, B.; Wan, Y.; Li, Y.C.; Yao, Y.; Zhang, S.; Xie, J. Activation of Humic Acid in Lignite Using Molybdate-Phosphorus Hierarchical Hollow Nanosphere Catalyst Oxidation: Molecular Characterization and Rice Seed Germination-Promoting Performances. *J. Agric. Food Chem.* **2020**, *68*, 13620–13631. [CrossRef]
19. Tang, Y.; Yang, Y.; Hou, S.; Cheng, D.; Yao, Y.; Zhang, S.; Xie, J.; Wang, X.; Ma, X.; Yu, Z.; et al. Multifunctional Iron–Humic Acid Fertilizer from Ball Milling Double-Shelled Fe–N-doped Hollow Mesoporous Carbon Microspheres with Lignite. *ACS Sustain. Chem. Eng.* **2021**, *9*, 717–731. [CrossRef]
20. Tang, Y.; Yang, Y.; Cheng, D.; Gao, B.; Wan, Y.; Li, Y.C.; Yao, Y.; Xie, J.; Liu, L. Multifunctional Slow-Release Fertilizer Prepared from Lignite Activated by a 3D-Molybdate-Sulfur Hierarchical Hollow Nanosphere Catalyst. *ACS Sustain. Chem. Eng.* **2019**, *7*, 10533–10543.
21. Xu, X.; Wang, W.; Zhou, W.; Shao, Z. Recent Advances in Novel Nanostructuring Methods of Perovskite Electrocatalysts for Energy-Related Applications. *Small Methods* **2018**, *2*, 1800071. [CrossRef]
22. Meng, Q.; Wang, W.; Weng, X.; Liu, Y.; Wang, H.; Wu, Z. Active Oxygen Species in La$_{n+1}$NinO$_{3n+1}$ Layered Perovskites for Catalytic Oxidation of Toluene and Methane. *J. Phys. Chem. C* **2016**, *120*, 3259–3266. [CrossRef]
23. Li, W.; Wang, S.; Li, J. Highly Effective Ru/BaCeO$_3$ Catalysts on Supports with Strong Basic Sites for Ammonia Synthesis. *Chem. Asian J.* **2019**, *14*, 2815–2821. [PubMed]
24. Zhu, J.; Li, H.; Zhong, L.; Xiao, P.; Xu, X.; Yang, X.; Zhao, Z.; Li, J. Perovskite Oxides: Preparation, Characterizations, and Applications in Heterogeneous Catalysis. *ACS Catal.* **2014**, *4*, 2917–2940. [CrossRef]
25. Liu, J.; Zhao, Z.; Xu, C.-M.; Duan, A.-J.; Jiang, G.-Y. The Structures, Adsorption Characteristics of La−Rb−Cu−O Perovskite-like Complex Oxides, and Their Catalytic Performances for the Simultaneous Removal of Nitrogen Oxides and Diesel Soot. *J. Phys. Chem. C* **2008**, *112*, 5930–5941. [CrossRef]
26. Nair, M.M.; Kaliaguine, S.; Kleitz, F. Nanocast LaNiO$_3$ Perovskites as Precursors for the Preparation of Coke-Resistant Dry Reforming Catalysts. *ACS Catal.* **2014**, *4*, 3837–3846. [CrossRef]
27. Xiao, G.; Xin, S.; Wang, H.; Zhang, R.; Wei, Q.; Lin, Y. Catalytic Oxidation of Styrene over Ce-Substituted La$_{1-x}$Ce$_x$MnO$_3$ Catalysts. *Ind. Eng. Chem. Res.* **2019**, *58*, 5388–5396. [CrossRef]

28. Zhang, C.; Guo, Y.; Guo, Y.; Lu, G.; Boreave, A.; Retailleau, L.; Baylet, A.; Giroir-Fendler, A. LaMnO$_3$ perovskite oxides prepared by different methods for catalytic oxidation of toluene. *Appl. Catal. B: Environ.* **2014**, *148*, 490–498. [CrossRef]

29. Liu, J.; Jia, E.; Wang, L.; Stoerzinger, K.A.; Zhou, H.; Tang, C.S.; Yin, X.; He, X.; Bousquet, E.; Bowden, M.E.; et al. Tuning the Electronic Structure of LaNiO$_3$ through Alloying with Strontium to Enhance Oxygen Evolution Activity. *Adv. Sci.* **2019**, *6*, 1901073. [CrossRef]

30. Kubota, K.; Pang, Y.D.; Miura, A.; Ito, H. Redox reactions of small organic molecules using ball milling and piezoelectric materials. *Science* **2019**, *366*, 1500–1504. [CrossRef]

31. Ohtomo, A.; Hwang, H.Y. A high-mobility electron gas at the LaAlO3/SrTiO3 heterointerface. *Nature* **2004**, *427*, 423–4266. [CrossRef] [PubMed]

32. Arandiyan, H.; Li, J.; Ma, L.; Hashemnejad, S.M.; Mirzaei, M.Z.; Chen, J.; Chang, H.; Liu, C.; Wang, C.; Chen, L. Methane reforming to syngas over LaNi$_x$Fe$_{1-x}$O$_3$ ($0 \leq x \leq 1$) mixed-oxide perovskites in the presence of CO$_2$ and O$_2$. *J. Ind. Eng. Chem.* **2012**, *18*, 2103–2114. [CrossRef]

33. Mickevičius, S.; Grebinskij, S.; Bondarenka, V.; Vengalis, B.; Šliužienė, K.; Orlowski, B.A.; Osinniy, V.; Drube, W. Investigation of epitaxial LaNiO$_{3-x}$ thin films by high-energy XPS. *J. Alloys Compd.* **2006**, *423*, 107–111. [CrossRef]

34. Peng, C.; Rao, C.; Ji, Y.; Zhang, L.; Liu, W.; Wang, X.; Xu, X.; Wang, Z.; Zhang, N.; Peng, H. Double-shelled hollow LaNiO$_3$ nanocage as nanoreactors with remarkable catalytic performance: Illustrating the special morphology and performance relationship. *Mol. Catal.* **2018**, *455*, 57–67. [CrossRef]

35. Zheng, Y.; Li, K.; Wang, H.; Wang, Y.; Tian, D.; Wei, Y.; Zhu, X.; Zeng, C.; Luo, Y. Structure dependence and reaction mechanism of CO oxidation: A model study on macroporous CeO$_2$ and CeO$_2$-ZrO$_2$ catalysts. *J. Catal.* **2016**, *344*, 365–377. [CrossRef]

36. Fu, C.; He, D.; Wang, Y.; Zhao, X. Facile synthesis and microwave absorption performance of coated carbon nanotubes by porous Fe$_3$O$_4$@C nanorods. *Synthetic Met.* **2019**, *248*, 76–80. [CrossRef]

37. Zheng, T.; Liang, Y.; Ye, S.; He, Z. Superabsorbent hydrogels as carriers for the controlled-release of urea: Experiments and a mathematical model describing the release rate. *Biosyst. Eng.* **2009**, *102*, 44–50. [CrossRef]

38. Oliveira, L.K.; Molina, E.F.; Moura, A.L.; de Faria, E.H.; Ciuffi, K.J. Synthesis, Characterization, and Environmental Applications of Hybrid Materials Based on Humic Acid Obtained by the Sol-Gel Route. *ACS Appl. Mater. Inter.* **2016**, *8*, 1478–1485. [CrossRef]

39. Kozyatnyk, I.; Lövgren, L.; Tysklind, M.; Haglund, P. Multivariate assessment of barriers materials for treatment of complex groundwater rich in dissolved organic matter and organic and inorganic contaminants. *J. Environ. Chem. Eng.* **2017**, *5*, 3075–3082. [CrossRef]

40. Tatzber, M.; Stemmer, M.; Spiegel, H.; Katzlberger, C.; Haberhauer, G.; Mentler, A.; Gerzabek, M.H. FTIR-spectroscopic characterization of humic acids and humin fractions obtained by advanced NaOH, Na$_4$P$_2$O$_7$, and Na$_2$CO$_3$ extraction procedures. *J. Plant Nutr. Soil Sci.* **2007**, *170*, 522–529. [CrossRef]

41. Skripkina, T.S.; Bychkov, A.L.; Tikhova, V.D.; Lomovsky, O.I. Mechanochemical Solid-Phase Reactions of Humic Acids from Brown Coal with Sodium Percarbonate. *Solid Fuel Chem.* **2019**, *52*, 356–360. [CrossRef]

42. Kozyatnyk, I.; Latham, K.G.; Jansson, S. Valorization of Humic Acids by Hydrothermal Conversion into Carbonaceous Materials: Physical and Functional Properties. *ACS Sustain. Chem. Eng.* **2018**, *7*, 2585–2592. [CrossRef]

43. Baglieri, A.; Vindrola, D.; Gennari, M.; Negre, M. Chemical and spectroscopic characterization of insoluble and soluble humic acid fractions at different pH values. *Chem. Biol. Technol. Agric.* **2014**, *1*, 9. [CrossRef]

44. Monteil-Rivera, F.; Brouwer, E.B.; Masset, S.; Deslandes, Y.; Dumonceau, J. Combination of X-ray photoelectron and solid-state ^{13}C nuclear magnetic resonance spectroscopy in the structural characterisation of humic acids. *Anal. Chim. Acta* **2000**, *424*, 243–255. [CrossRef]

45. Doskočil, L.; Burdíková-Szewieczková, J.; Enev, V.; Kalina, L.; Wasserbauer, J. Spectral characterization and comparison of humic acids isolated from some European lignites. *Fuel* **2018**, *213*, 123–132. [CrossRef]

46. Jing, Q.; Li, H. Hierarchical nickel cobalt oxide spinel microspheres catalyze mineralization of humic substances during wet air oxidation at atmospheric pressure. *Appl. Catal. B Environ.* **2019**, *256*, 117858. [CrossRef]

47. Wang, M.; Cui, S.; Yang, X.; Bi, W. Synthesis of g-C$_3$N$_4$/Fe$_3$O$_4$ nanocomposites and application as a new sorbent for solid phase extraction of polycyclic aromatic hydrocarbons in water samples. *Talanta* **2015**, *132*, 922–928. [CrossRef]

48. Campitelli, P.A.; Velasco, M.I.; Ceppi, S.B. Chemical and physicochemical characteristics of humic acids extracted from compost, soil and amended soil. *Talanta* **2006**, *69*, 1234–1239. [CrossRef]